Scattering by rotationally symmetric anisotropic spheres: Potential formulation and parametric studies

Cheng-Wei Qiu,* Le-Wei Li,† and Tat-Soon Yeo
Department of Electrical and Computer Engineering, National University of Singapore, Kent Ridge, Singapore 119260

Saïd Zouhdi
Laboratoire de Génie Electrique de Paris, Ecole Supérieure D'Électricité, Plateau de Moulon 91192, Gif-Sur-Yvette, Cedex, France
(Received 18 April 2006; published 13 February 2007)

Vector potential formulation and parametric studies of electromagnetic scattering problems of a sphere characterized by the rotationally symmetric anisotropy are studied. Both $\bar{\epsilon}$ and $\bar{\mu}$ tensors are considered herein, and four elementary parameters are utilized to specify the material properties in the structure. The field representations can be obtained in terms of two potentials, and both TE (TM) modes (with respect to $\hat{r}$) inside (outside) the sphere can be derived and expressed in terms of a series of fractional-order (in a real or complex number) Ricatti-Bessel functions. The effects due to either electric anisotropy ratio ($A_e=\epsilon_t/\epsilon_r$) or magnetic anisotropy ratio ($A_m=\mu_t/\mu_r$) on the radar cross section (RCS) are considered, and the hybrid effects due to both A_e and A_m are also examined extensively. It is found that the material anisotropy affects significantly the scattering behaviors of three-dimensional dielectric objects. For absorbing spheres, however, the A_e or A_m no longer plays a significant role as in lossless dielectric spheres and the anisotropic dependence of RCS values is found to be predictable. The hybrid effects of A_e and A_m are considered for absorbing spheres as well, but it is found that the RCS can be greatly reduced by controlling the material parameters. Details of the theoretical treatment and numerical results are presented.

DOI: 10.1103/PhysRevE.75.026609 PACS number(s): 03.50.De, 41.20.Jb, 42.25.Bs, 52.40.Db

I. INTRODUCTION

Due to recent advances in material science and technology and increasing applications of anisotropic materials for microstrip circuits and microwave engineering, analysis and characterization of electromagnetic interactions with anisotropic materials have been a subject of great interest in recent years. Among those investigations in the literature, scattering of electromagnetic waves by anisotropic three-dimensional (3D) objects has attracted considerable attention [1,2]. In the analysis of scattering problems associated with anisotropic media, the 3D Fourier transform technique was widely used [3,4] to relate the space and spectral domains and this is especially true for waves and fields in planar multilayered structures. The Lorenz-Mie analytical approach is an important theory and is usually employed [5–7] especially when the problem geometry is of spherical and radially layered configurations. The method of angular spectrum expansion is also often applied to provide a coordinate transformation [8]. The dyadic Green's function technique [9] is a powerful analytic method for solving boundary-value problems and is a kernel for the integral equation necessary for the method of moments and the boundary element method. Scattering by inhomogeneous 3D objects is treated by the method of separation of variables [10] in spheroidal coordinates and by extending the Lorenz-Mie theory to spherically multilayered cases [11], and scattering by periodical spherical structures [12] and gyrotropic spheres [13,14] are studied as well.

For most of these published works, however, investigations of the scattering behaviors of anisotropic media are carried out by considering only planar geometry [15–17] or cylindrical structures [18–20]. Due to the mathematical complexity of studying spherical anisotropic objects, some studies have been done and progress has been made in the analysis of 3D anisotropic objects recently, which only focused on field expressions [21,22] using the method of moments [23], the second-harmonic generation approach [24], and the coupled-dipole methods [25]. As far as we know, little work has been done so far on parametric studies of the material anisotropy effects on the scattering performance in spherical coordinate system or spherical anisotropic 3D objects with both electric and magnetic anisotropic properties. So far, there is no reported process to fabricate such anisotropic materials, but such materials are likely to be fabricated in the future especially with the fast advancement of nanoscience and nanotechnology. The theorem developed in this paper will be very useful and helpful especially in engineering those uniaxial materials. Also, it provides us some ideas to control (by minimizing and maximizing) the radar cross sections (RCS's) if unintentional uniaxial anisotropy in the surface of the material is introduced during the manufacturing process.

In this paper, field expansions in all regions due to an incident plane wave propagating in the presence of anisotropic spheres are made using potentials with TE and TM decompositions. The scattered field and total field can be thus obtained by imposing boundary conditions at the sphere surface and using the superposition technique, respectively. The parametric studies are of particular interest in this paper, from which we can find how the RCS's will be affected and

*Also with Laboratoire de Génie Electrique de Paris, Ecole Supérieure D'Électricité, Plateau de Moulon 91192, Gif-Sur-Yvette, France.
†Corresponding author. Electronic address: lwli@nus.edu.sg

 ©2007 The American Physical Society

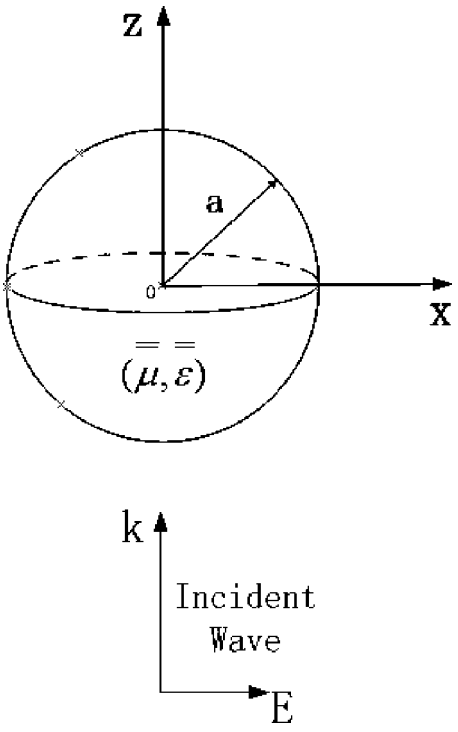

FIG. 1. Geometry of scattering of a plane wave by an anisotropic sphere.

what we could do to control of the RCS values. To gain physical insight, the RCS results are studied for a wide range of joint anisotropy (A_e and A_m), and compared to the results of both the isotropic case and the single-anisotropy (only A_e or A_m) case. It is worthwhile to note that RCS's will exhibit some new characteristics in joint anisotropy cases and we also construct a general expression $|\frac{\sqrt{\mu_r}-\sqrt{\epsilon_t}}{\sqrt{\mu_r}+\sqrt{\epsilon_t}}|^2$ to predict RCS's for anisotropic spheres, which will be of great use in radar detection and military purposes. It is of major interest to know how significantly anisotropy influences electromagnetic scattering, so that we can adjust the parameters of the 3D objects to control the RCS values, either for enhancement or for reduction.

II. POTENTIAL FORMULATION AND FIELD EXPANSIONS

In this paper, electromagnetic scattering of a plane wave by an anisotropic sphere (as shown in Fig. 1) is treated, where the material parameters are characterized by constitutive tensors of permittivity and permeability to be specified later. For anisotropic media, the constitutive relationships as used in the Maxwell equations are

$$\nabla \times \boldsymbol{E} = -i\omega\bar{\boldsymbol{\mu}} \cdot \boldsymbol{H}, \tag{1}$$

$$\nabla \times \boldsymbol{H} = i\omega\bar{\boldsymbol{\epsilon}} \cdot \boldsymbol{E} + \boldsymbol{J}, \tag{2}$$

where the time dependence $e^{i\omega t}$ has been assumed but suppressed. Consider an anisotropic sphere of radius a located at the origin of a coordinate system as shown in Fig. 1. The constitutive relations are given by

$$\bar{\boldsymbol{\epsilon}} = \epsilon_0 \begin{bmatrix} \epsilon_r & 0 & 0 \\ 0 & \epsilon_t & 0 \\ 0 & 0 & \epsilon_t \end{bmatrix}, \tag{3}$$

$$\bar{\boldsymbol{\mu}} = \mu_0 \begin{bmatrix} \mu_r & 0 & 0 \\ 0 & \mu_t & 0 \\ 0 & 0 & \mu_t \end{bmatrix}, \tag{4}$$

where the identity dyadic is expressed as $\bar{\boldsymbol{I}} = \hat{\boldsymbol{r}}\hat{\boldsymbol{r}} + \hat{\boldsymbol{\theta}}\hat{\boldsymbol{\theta}} + \hat{\boldsymbol{\phi}}\hat{\boldsymbol{\phi}}$ and ϵ (or μ) is the permittivity (or permeability), and ϵ_r (or μ_r) and ϵ_t (or μ_t) stand for the relative permittivities (or permeabilities) perpendicular and parallel to the sphere surface, respectively. In an alternative form, we can rewrite Eqs. (1) and (2) as

$$\nabla \times (\bar{\boldsymbol{\epsilon}}^{-1} \cdot \boldsymbol{D}) = -i\omega\boldsymbol{B}, \tag{5}$$

$$\nabla \times (\bar{\boldsymbol{\mu}}^{-1} \cdot \boldsymbol{B}) = i\omega\boldsymbol{D} + \boldsymbol{J}. \tag{6}$$

Considering the source-free case of the equations above with the vector identities, we can express $\boldsymbol{B}$ and $\boldsymbol{D}$ in terms of the following two sets of scalar eigenfunctions:

$$\boldsymbol{B}_{\mathrm{TM}} = \nabla \times (\hat{\boldsymbol{r}}\psi_{\mathrm{TM}}), \tag{7}$$

$$\boldsymbol{D}_{\mathrm{TE}} = -\nabla \times (\hat{\boldsymbol{r}}\psi_{\mathrm{TE}}), \tag{8}$$

where ψ_{TE} and ψ_{TM} denote potentials for the TM and TE modes, considered with respect to $\hat{\boldsymbol{r}}$ in the spherical coordinate system.

Substituting Eqs. (7) and (8) into Eqs. (5) and (6), we obtain

$$\boldsymbol{B}_{\mathrm{TE}} = \frac{1}{i\omega}\{\nabla \times [\bar{\boldsymbol{\epsilon}}^{-1} \cdot \nabla \times (\hat{\boldsymbol{r}}\psi_{\mathrm{TE}})]\}, \tag{9}$$

$$\boldsymbol{D}_{\mathrm{TM}} = \frac{1}{i\omega}\{\nabla \times [\bar{\boldsymbol{\mu}}^{-1} \cdot \nabla \times (\hat{\boldsymbol{r}}\psi_{\mathrm{TM}})]\}. \tag{10}$$

After some manipulations of those equations regarding $\boldsymbol{B}$ and $\boldsymbol{D}$, we obtain

$$\frac{\epsilon_r}{\epsilon_t}\frac{\partial^2\psi_{\mathrm{TM}}}{\partial r^2} + \frac{1}{r^2\sin\theta}\frac{\partial}{\partial\theta}\left(\sin\theta\frac{\partial\psi_{\mathrm{TM}}}{\partial\theta}\right) + \frac{1}{r^2\sin^2\theta}\frac{\partial^2\psi_{\mathrm{TM}}}{\partial\phi^2} + \omega^2\mu_0\epsilon_0\mu_t\epsilon_r\psi_{\mathrm{TM}} = 0, \tag{11}$$

$$\frac{\mu_r}{\mu_t}\frac{\partial^2\psi_{\mathrm{TE}}}{\partial r^2} + \frac{1}{r^2\sin\theta}\frac{\partial}{\partial\theta}\left(\sin\theta\frac{\partial\psi_{\mathrm{TE}}}{\partial\theta}\right) + \frac{1}{r^2\sin^2\theta}\frac{\partial^2\psi_{\mathrm{TE}}}{\partial\phi^2} + \omega^2\mu_0\epsilon_0\mu_r\epsilon_t\psi_{\mathrm{TE}} = 0. \tag{12}$$

It can be seen that in the case of $\epsilon_r = \epsilon_t$ and $\mu_r = \mu_t$, the above equations are reduced to the results of isotropic media [26].

Using the separation of variables method, we find that the solutions to the above equations are composed of superpositions of Ricatti-Bessel functions, associated Legendre polynomials, and trigonometric functions—i.e.,

$$\psi_{\mathrm{TM}} = \sum_{m,n} a_{m,n} j_{v_1}(k_t r) P_n^m(\cos\theta) \begin{matrix}\cos \\ \sin\end{matrix} m\phi, \tag{13}$$

$$\psi_{\mathrm{TE}} = \sum_{m,n} b_{m,n} j_{v_2}(k_t r) P_n^m(\cos\theta) \begin{matrix}\cos\\ \sin\end{matrix} m\phi, \tag{14}$$

$$v_1 = \left[n(n+1)A_e + \frac{1}{4} \right]^{1/2} - \frac{1}{2}, \tag{15}$$

$$v_2 = \left[n(n+1)A_m + \frac{1}{4} \right]^{1/2} - \frac{1}{2}, \tag{16}$$

$$k_t = \omega\sqrt{\epsilon_0 \mu_0 \epsilon_t \mu_t}, \tag{17}$$

where $A_e = \epsilon_t/\epsilon_r$ and $A_m = \mu_t/\mu_r$ represent the electric and magnetic anisotropy ratios, respectively, $a_{m,n}$ and $b_{m,n}$ denote the expansion coefficients, and v_1 and v_2 stand for the orders of spherical Ricatti-Bessel functions which can be complex in value. Thus, the field expansions in spherical coordinates can be obtained using the TE and TM decompositions

$$E_r = \frac{\omega}{ik_t^2}\left(\frac{\partial^2}{\partial r^2} + k_t^2 \right)\psi_{\mathrm{TM}}, \tag{18}$$

$$E_\theta = \frac{-1}{\epsilon_0 \epsilon_t r \sin\theta}\frac{\partial \psi_{\mathrm{TE}}}{\partial \phi} + \frac{\omega}{ik_t^2 r}\frac{\partial^2 \psi_{\mathrm{TM}}}{\partial r \partial \theta}, \tag{19}$$

$$E_\phi = \frac{1}{\epsilon_0 \epsilon_t r}\frac{\partial \psi_{\mathrm{TE}}}{\partial \theta} + \frac{\omega}{ik_t^2 r \sin\theta}\frac{\partial^2 \psi_{\mathrm{TM}}}{\partial r \partial \phi}, \tag{20}$$

$$H_r = \frac{\omega}{ik_t^2}\left(\frac{\partial^2}{\partial r^2} + k_t^2 \right)\psi_{\mathrm{TE}}, \tag{21}$$

$$H_\theta = \frac{\omega}{ik_t^2 r}\frac{\partial^2 \psi_{\mathrm{TE}}}{\partial r \partial \theta} + \frac{1}{\mu_0 \mu_t r \sin\theta}\frac{\partial \psi_{\mathrm{TM}}}{\partial \phi}, \tag{22}$$

$$H_\phi = \frac{\omega}{ik_t^2 r \sin\theta}\frac{\partial^2 \psi_{\mathrm{TE}}}{\partial r \partial \phi} - \frac{1}{\mu_0 \mu_t r}\frac{\partial \psi_{\mathrm{TM}}}{\partial \theta}. \tag{23}$$

As we can see, the wave propagation is dependent on both A_e and A_m.

III. SCATTERED FIELD AND RCS's

We notice that if the nondiagonal components of the material tensors $\bar{\boldsymbol{\epsilon}}$ and $\bar{\boldsymbol{\mu}}$ are zero, then the rotations would be equivalent to letting $\hat{\boldsymbol{r}}\hat{\boldsymbol{r}}$ be unchanged while rotating the transverse elements (to $\hat{\boldsymbol{r}}$) with $\hat{\boldsymbol{r}}$ as axes. The material in our study remains invariant under such a rotation, which was called G type [27] where the analysis was in 2D with respect to $\hat{z}$ as the axis of rotation. In that case, G type is referred to $\hat{z}$. If we extend that to the present G type with respect to $\hat{\boldsymbol{r}}$, we can have the characterization for anisotropic material tensors in spherical coordinates (r, θ, ϕ).

For absorbing spheres, the elements in $\bar{\boldsymbol{\epsilon}}$ and $\bar{\boldsymbol{\mu}}$, or at least one of these two tensors, are complex in value. A plane wave, as shown in Fig. 1, is characterized by

$$\boldsymbol{E}_i = \hat{\boldsymbol{x}} e^{-ik_0 r\cos\theta}, \tag{24}$$

$$\boldsymbol{H}_i = \hat{\boldsymbol{y}}\sqrt{\frac{\epsilon_0}{\mu_0}} e^{-ik_0 r\cos\theta}, \tag{25}$$

where a unity amplitude of the incident wave propagating upon the sphere is assumed. To match the boundary conditions at the surface of the sphere, the exponential terms in the above equations can be expanded in terms of spherical harmonics by employing the following identity:

$$e^{-ik_0 r\cos\theta} = \sum_{n=0}^{\infty} \frac{i^{-n}(2n+1)}{k_0 r} j_n(k_0 r) P_n(\cos\theta). \tag{26}$$

By equating the radial components in Eqs. (24) and (25) to those in Eqs. (18)–(23), the scalar functions of ψ_{TE}^i and ψ_{TM}^i for incident fields can be expressed as

$$\psi_{\mathrm{TE}}^i = \frac{\sin\phi}{\omega\eta_0}\sum_{n=1}^{\infty} \frac{i^{-n}(2n+1)}{n(n+1)} j_n(k_0 r) P_n^1(\cos\theta), \tag{27}$$

$$\psi_{\mathrm{TM}}^i = \frac{\cos\phi}{\omega}\sum_{n=1}^{\infty} \frac{i^{-n}(2n+1)}{n(n+1)} j_n(k_0 r) P_n^1(\cos\theta). \tag{28}$$

Similarly, ψ_{TE}^s and ψ_{TM}^s for scattered fields can be thus derived to be

$$\psi_{\mathrm{TE}}^s = \frac{\sin\phi}{\omega\eta_0}\sum_{n=1}^{\infty} b_n h_n^{(2)}(k_0 r) P_n^1(\cos\theta a), \tag{29}$$

$$\psi_{\mathrm{TM}}^s = \frac{\cos\phi}{\omega}\sum_{n=1}^{\infty} a_n h_n^{(2)}(k_0 r) P_n^1(\cos\theta), \tag{30}$$

where $j_n(\cdot)$ and $h_n^{(2)}(\cdot)$ denote first-kind spherical Bessel and second-kind Hankel functions, respectively. Then, ψ_{TE}^t and ψ_{TM}^t for the transmitted fields inside the sphere can be reduced to

$$\psi_{\mathrm{TE}}^t = \frac{\sin\phi}{\omega\eta_0}\sum_{n=1}^{\infty} d_n j_{v_2}(k_t r) P_n^1(\cos\theta), \tag{31}$$

$$\psi_{\mathrm{TM}}^t = \frac{\cos\phi}{\omega}\sum_{n=1}^{\infty} c_n j_{v_1}(k_t r) P_n^1(\cos\theta), \tag{32}$$

where a_n, b_n, c_n, and d_n are unknown expansion coefficients to be determined by matching the boundary conditions which require continuity of the tangential components of the electromagnetic fields on the surface at $r=a$. Normally, there are four sets of boundary equations

$$E_\theta^t(a) = E_\theta^i(a) + E_\theta^s(a), \tag{33}$$

$$E_\phi^t(a) = E_\phi^i(a) + E_\phi^s(a), \tag{34}$$

$$H_\theta^t(a) = H_\theta^i(a) + H_\theta^s(a), \tag{35}$$

$$H_\phi^t(a) = H_\phi^i(a) + H_\phi^s(a). \tag{36}$$

Actually, after careful examination, it is found that only two sets of equations (33) and (35) or the other two sets of equa-

tions (34) and (36) are sufficient enough to determine those expansion coefficients. These coefficients are obtained and given as

$$a_n = \frac{\sqrt{\mu_t/\epsilon_t} j_n(k_0 a) j'_{v_1}(k_t a) - j'_n(k_0 a) j_{v_1}(k_t a)}{h_n^{(2)'}(k_0 a) j_{v_1}(k_t a) - \sqrt{\mu_t/\epsilon_t} h_n^{(2)}(k_0 a) j'_{v_1}(k_t a)} T_n, \quad (37)$$

$$b_n = \frac{\sqrt{\mu_t/\epsilon_t} j'_n(k_0 a) j_{v_2}(k_t a) - j_n(k_0 a) j'_{v_2}(k_t a)}{h_n^{(2)}(k_0 a) j'_{v_2}(k_t a) - \sqrt{\mu_t/\epsilon_t} h_n^{(2)'}(k_0 a) j_{v_2}(k_t a)} T_n, \quad (38)$$

$$c_n = \frac{i}{\sqrt{\mu_t/\epsilon_t} h_n^{(2)}(k_0 a) j'_{v_1}(k_t a) - h_n^{(2)'}(k_0 a) j_{v_1}(k_t a)} T_n, \quad (39)$$

$$d_n = \frac{i\sqrt{\mu_t/\epsilon_t}}{h_n^{(2)}(k_0 a) j'_{v_2}(k_t a) - \sqrt{\mu_t/\epsilon_t} h_n^{(2)'}(k_0 a) j_{v_2}(k_t a)} T_n, \quad (40)$$

$$T_n = \frac{i^{-n}(2n+1)}{n(n+1)}, \quad (41)$$

where Wronskians for spherical pairs of solutions are employed herewith. The derivative in the above equations is taken with respect to the argument (i.e., $\partial[j_n(x)]/\partial x$). With these coefficients solved, the field components of the scattered, transmitted, and total fields can be obtained by corresponding substitutions. Of particular interest is the backscattered field, from which we can calculate the RCS:

$$A_{xx} = \lim_{r\to\infty}\left(4\pi r^2 \frac{|E_x^s|^2}{|E_x^i|^2}\right). \quad (42)$$

IV. NUMERICAL RESULTS

In this section, we mainly focus on the following two areas: that is, the effects of (i) dielectric spheres and (ii) absorbing spheres. For each area, typical results for (a) single electric and magnetic anisotropy effects, (b) joint anisotropy effects, and (c) RCS prediction on the RCS values will be studied in a wide range. In all the following RCS calculations, the truncation of the summations is chosen to be 50, at which the convergence has been verified to be acceptable.

A. Dielectric spheres

For dielectric spheres, all elements in $\bar{\epsilon}$ and $\bar{\mu}$ are real values. First, we consider the RCS results for isotropic sphere as shown in Fig. 2.

In Fig. 2, it is shown that these two curves agree quite well for dielectric spheres ($v_1 = v_2 = n$) where there is actually no difference theoretically. Further simulation results show that the backscattering behaviors are the same for these two dielectric spheres (ϵ_1 and μ_1 for the first case, ϵ_2 and μ_2 for the second case) only if $\sqrt{\epsilon_1\mu_1} = \sqrt{\epsilon_2\mu_2}$ and $\sqrt{\mu_1/\epsilon_1} = 1/\sqrt{\mu_2/\epsilon_2}$. It can be also verified by observation in Eqs. (37) and (38). In the calculation of the backscattering RCS (A_{xx}) of spheres, the expression will be in the form of a summation and each term will have $b_n - a_n$. Under the conditions of $\sqrt{\epsilon_1\mu_1} = \sqrt{\epsilon_2\mu_2}$ and $\sqrt{\mu_1/\epsilon_1} = 1/\sqrt{\mu_2/\epsilon_2}$, each summation term of $b_n - a_n$ for those two dielectric spheres will only have a sign change, but the final expression in Eq. (3) will not change since it is dependent on the absolute value of $b_n - a_n$. Later, we will compare the results of the following anisotropic cases with those of the isotropic case so as to find out the rules of RCS dependence prediction.

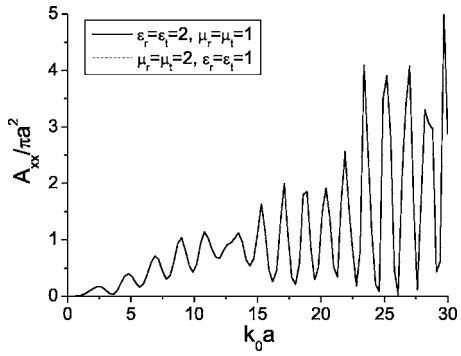

FIG. 2. Normalized RCS values versus $k_0 a$ of an isotropic sphere.

1. Electric and magnetic anisotropy effects

For uniaxial ferrite spheres, we assume that $\epsilon_r = \epsilon_t = 1$ applies to all cases in Fig. 3. In Fig. 3(a), the RCS values due to a negative uniaxial sphere ($\mu_r < \mu_t$) with $A_m = 1.2$, $A_m = 1.4$, and $A_m = 1.6$ are shown, while in Fig. 3(b), the RCS values due to a positive uniaxial sphere ($\mu_r > \mu_t$) with A_m

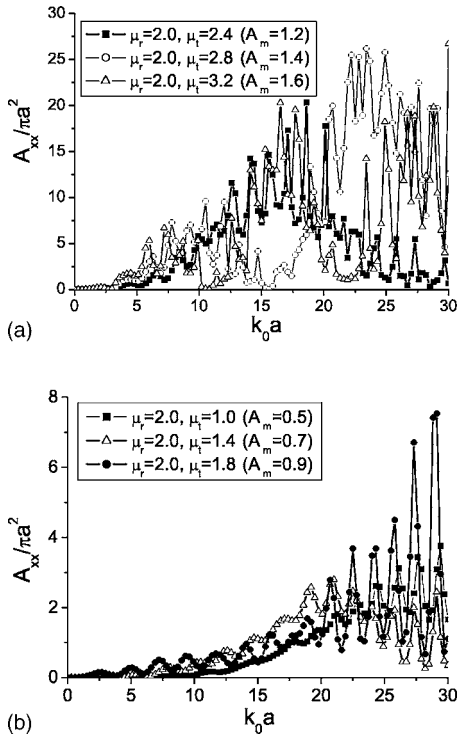

FIG. 3. Normalized RCS values versus $k_0 a$ for uniaxial ferrite spheres under the condition $\epsilon_r = \epsilon_t = 1$ (a) Negative uniaxial Ferrite spheres. (b) Positive uniaxial Ferrite spheres.

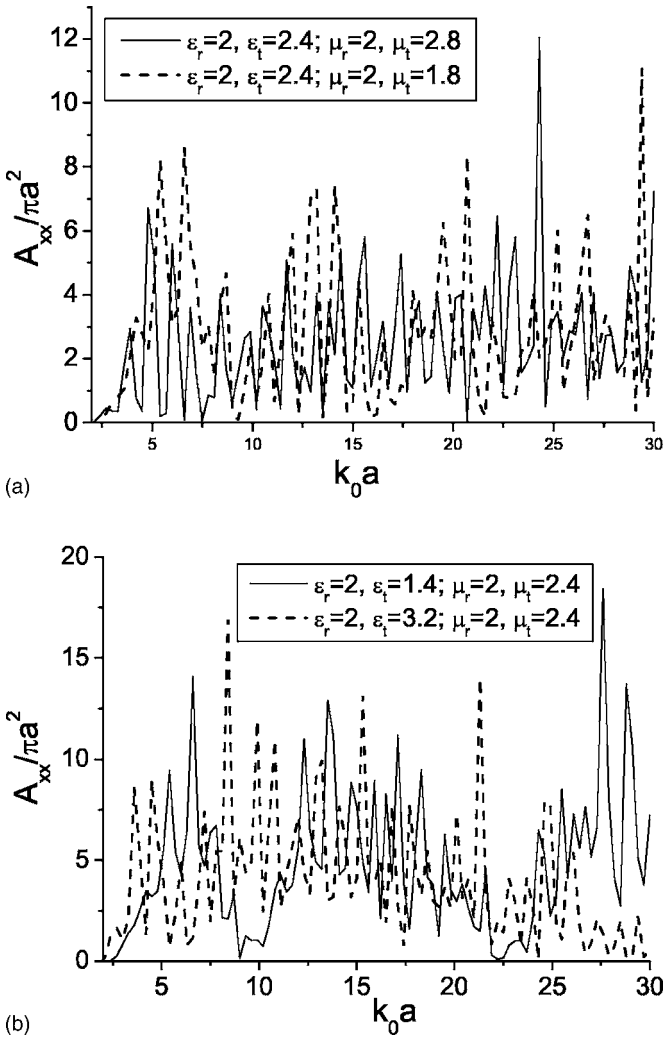

FIG. 4. Normalized RCS values versus k_0a for generalized anisotropic spheres. (a) Solid Curve: $A_e=1.2$, $A_m=1.4$; Dashed curve: $A_e=1.2$, $A_m=0.9$. (b) Solid Curve: $A_e=0.7$, $A_m=1.2$; Dashed curve: $A_e=1.6$, $A_m=1.2$.

$=0.9$, $A_m=0.7$, and $A_m=0.5$ are depicted. It is observed that the RCS values are quite sensitive to the anisotropy and the scattering characteristics of a dielectric sphere are greatly affected by the presence of anisotropy. In addition, the oscillation of the RCS values due to negative spheres is much sharper and more irregular than that due to positive spheres, and the oscillation range of RCS values of negative spheres is wider.

For electric anisotropic spheres, we assume that the condition of $\mu_r=\mu_t=1$ applies to all cases. After careful examination and simulation, it is found that the dependence of RCS's exhibits the same scattering performance with ferrite spheres in both negative and positive cases. Hence the figures of normalized RCS results for electric anisotropic spheres will not be given in detail due to length restrictions.

2. Hybrid anisotropy effect

In this case where $\epsilon_r \neq \epsilon_t$ and $\mu_r \neq \mu_t$, the hybrid effects due to A_e and A_m are of particular interest. In Fig. 4(a), we keep the $\bar{\epsilon}$ constant and change μ_r and μ_t so as to examine the anisotropy effect on the dependence of RCS values. By comparing Fig. 4 with Fig. 3, it is observed that under the same A_m, the RCS values are affected significantly by the existence of A_e, leading to hybrid anisotropy effects.

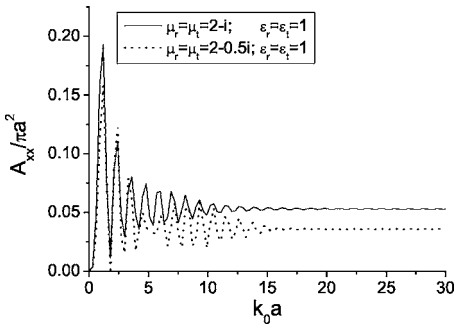

FIG. 5. Normalized RCS values versus k_0a for isotropic absorbing spheres.

3. RCS prediction

By comparing those results in Fig. 3 for uniaxial ferrite spheres with those in Fig. 4 for generalized anisotropic spheres and in Fig. 2 for isotropic spheres, it can be concluded that (a) the scattering performance of a dielectric sphere is significantly affected by the presence of anisotropy of the sphere, and (b) by studying many other different cases for a wide range of anisotropy effects, it is obvious that the dependence of RCS's on anisotropy is in a complex form and no general rules to predict the scattering behavior due to the anisotropy have been found in the present work. Therefore, control of the RCS values can be made by adjusting the factors or parameters in many different ways.

B. Absorbing spheres

In absorbing spheres, the elements of $\bar{\boldsymbol{\epsilon}}$ and $\bar{\boldsymbol{\mu}}$ in Eqs. (3) and (4) are complex in value. The imaginary parts represent absorptions. Subsequently, we will first examine the characteristics of isotropic absorbing spheres. In the cases given in Fig. 5, the orders of Bessel functions (i.e., v_1 and v_2) in Eqs. (13) and (14) are still integers. Figure 5 shows that for sufficiently large isotropic absorbing spheres ($k_0a>17$), normalized RCS values steadily approach 0.0529 and 0.0357 for solid and dashed curves, respectively. For small values of k_0a, a high oscillation would be present, and these results are comparable with the diagrams given in [1]. This fact thus confirms the validity of our theoretical formulation.

1. Electric and magnetic anisotropy effects

In this section, it is assumed that $\epsilon_r=\epsilon_t=1$ for all single-anisotropy cases. In Fig. 6(a), the RCS results for negative absorbing spheres ($\mu_r<\mu_t$) with $A_m=1.3-0.1i$, $A_m=1.4-0.3i$, and $A_m=1.5-0.5i$ are shown. It can be observed that when $k_0a>15$, all three curves approach their own constant values 0.08665, 0.1088, and 0.1325, respectively. It is noted that the periods and limits of damped oscillations which occur for $k_0a<5$ exhibit an irregular form, and for

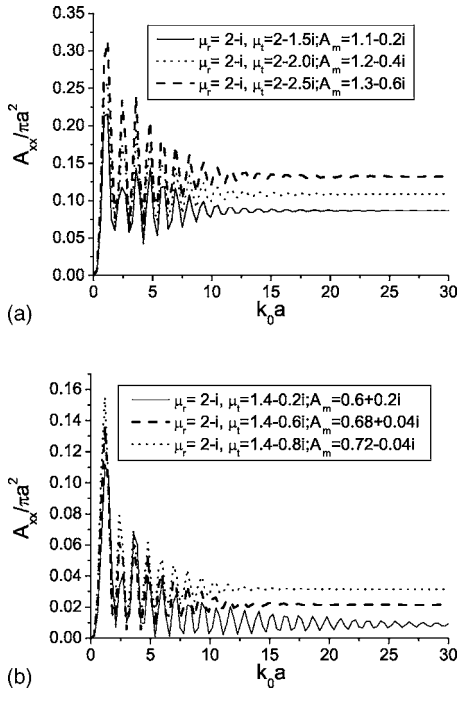

FIG. 6. Normalized RCS values versus k_0a for absorbing spheres when $\epsilon_r=\epsilon_t=1$ (a) Negative absorbing spheres. (b) Positive absorbing spheres.

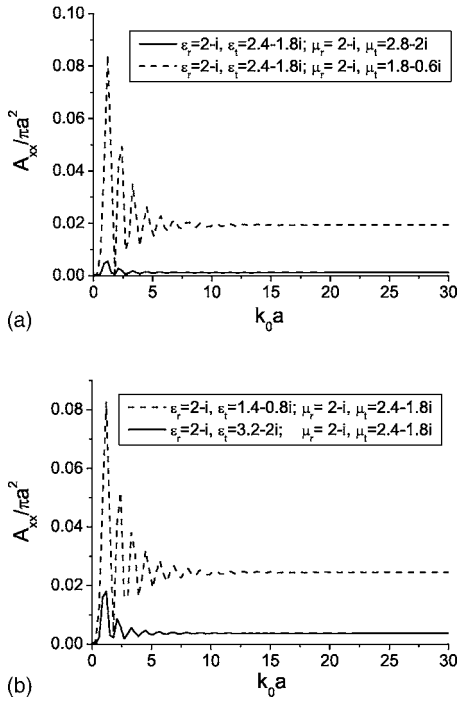

FIG. 7. Normalized RCS values versus k_0a for general absorbing spheres. (a) Solid Curve: $A_e=1.32-0.24i$ and $A_m=1.52-0.24i$; Dashed curve: $A_e=1.32-0.24i$ and $A_m=0.84+0.12i$. (b) Solid Curve: $A_e=1.68-1.16i$ and $A_m=1.32-0.24i$; Dashed curve: $A_e=0.72-0.04i$ and $A_m=1.32-0.24i$.

larger values of k_0a, the oscillations start to show a regular decaying form, which agrees with the results for isotropic cases for perfectly conducting spheres [1]. In Fig. 6(b), RCS values for positive absorbing spheres ($\mu_r>\mu_t$) in the three cases are shown. It exhibits characteristics of oscillation periods and limit values similar to those in Fig. 6(a); however, it can be seen that the higher the imaginary part of the complex permeability parallel to the spherical surface, the smaller the oscillation period for the region when $k_0a>5$. Higher absorption via the imaginary part in μ_t results in higher values of the limits of the damped oscillations. For practical purposes of RCS reductions, the positive absorbing spheres are preferred, since the backscattered field due to a positive absorbing sphere is only about one-fifth of the field due to a negative absorbing sphere.

2. Hybrid anisotropy effects

In this section, the A_e and A_m under consideration can be any complex numbers simultaneously assumed. It is worthwhile to note that some novel characteristics of RCS values will be presented. By comparing Fig. 7 with Fig. 4, it can be observed that the loss tangents or the imaginary parts of $\bar{\boldsymbol{\epsilon}}$ and $\bar{\boldsymbol{\mu}}$ significantly reduce the RCS values (almost hundreds of times) and also make the oscillation more flattened and predictable. This observation might be very useful in practical applications, especially in identifying aircraft coating materials which may generate some "invisible" effects.

Finally, we will obtain the RCS results for a special case where ϵ_r and μ_r can be arbitrary but $\epsilon_t=\mu_t$ As is shown in Figs. 8(a) and 8(b), for absorbing spheres (no matter of single or joint anisotropy), once the parallel permittivity equals parallel permeability, RCS values will approach zero in the region of $k_0a>3$ regardless of what ϵ_r and μ_r are. However, the dielectric sphere still shows an irregular fluctuation in Fig. 8(c) and the oscillations do not end up with a stable limit.

3. RCS prediction

From Fig. 5 to Fig. 8, it can be concluded that the transverse components of $\bar{\boldsymbol{\epsilon}}$ and $\bar{\boldsymbol{\mu}}$ dominate the scattering characteristics of absorbing spheres, which makes it possible to control the backscattering effects of anisotropy. We propose a general RCS prediction scheme here to calculate the limiting value of a damped oscillation in all figures in this section:

$$N_{\text{limit}}=\left|\frac{\sqrt{\frac{\mu_t}{\epsilon_t}}-1}{\sqrt{\frac{\mu_t}{\epsilon_t}}+1}\right|^2, \tag{43}$$

which is applicable to all sufficiently large absorbing spheres and can be reduced to the geometrical optics limit given in [28].

The physical insight here is that for a sufficiently large sphere, the electric vector of the incident plane wave is parallel to the boundary surface of the sphere. The permittivity ϵ_r and permeability μ_r, which are perpendicular to the electromagnetic perturbations of the incident wave, do not affect the backscattering behaviors. This phenomenon is due to the

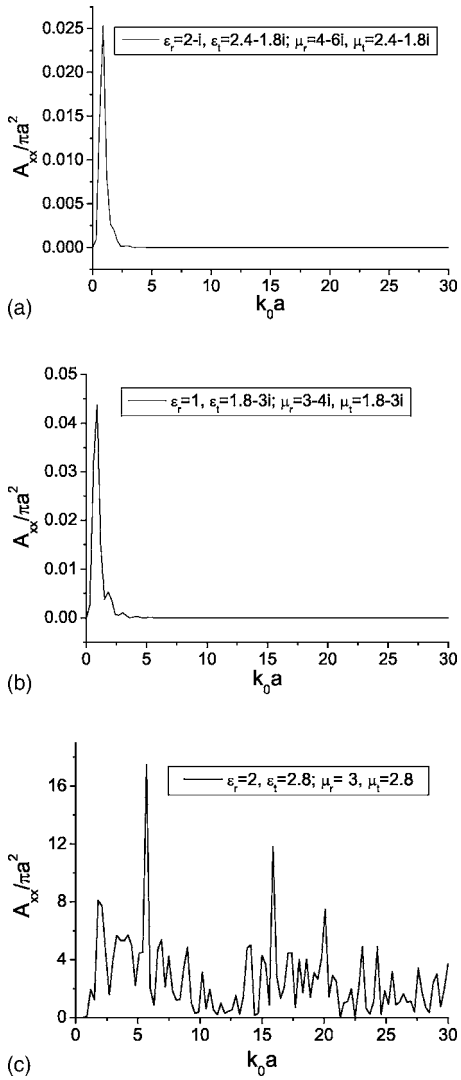

FIG. 8. Normalized RCS values versus k_0a for absorbing and dielectric spheres when $\epsilon_t=\mu_t$. (a) Absorbing sphere with $\epsilon_t=\mu_t=2.4-1.8i$. (b) Absorbing sphere with $\epsilon_t=\mu_t=1.8-3i$. (c) Absorbing sphere with $\epsilon_t=\mu_t=2.8$.

attenuation of the transmitted wave inside the absorbing spheres which causes all the scattering due to the reflection at the external boundary surface. If we use Eq. (43) to compute all limits of the figures, it is found that the theoretical results agree well with the numerical data.

V. CONCLUSIONS

In this paper, scattering by rotationally symmetric anisotropic spheres is studied extensively. Much effort has been spent not only in the formulation of potentials and TE- and TM-wave (with respect to $\hat{\boldsymbol{r}}$) decomposition, but also in the parametric studies of RCS characteristics. Calculated RCS values for an incident plane wave reveal that the existence of anisotropy significantly influences the scattering behavior of spherical objects. Furthermore, the hybrid anisotropy greatly affects the characteristics and dependence of RCS results more than a single anisotropy. If the material parameters are manipulated properly, the objects can be "transparent" to the detecting devices on the ground.

It is found that for the cases of dielectric spheres, the scattering behavior depends on the uniaxial anisotropy in a complex way. For the cases of absorbing spheres, however, the RCS values are affected primarily by the imaginary parts of the transverse component of $\bar{\boldsymbol{\epsilon}}$ and $\bar{\boldsymbol{\mu}}$; therefore, the dependence of backscattering RCS on single and joint anisotropies is found to be predictable. It is also observed that the RCS values approach a limit, which is determined by ϵ_t and μ_t, the permittivity and permeability elements parallel to the boundary surface. A determination of the limit of damped oscillations has been proposed in Eq. (43). Hence, if unintentional anisotropy is introduced due to natural reasons or due to the shear in the surface plan during processing, an absorbing material would be a better choice than a lossless dielectric material as a coating on a scatterer, and if single anisotropy exists, it will be much better to utilize the hybrid anisotropy to minimize or control the scattering behaviors further.

This paper, therefore, not only derives an analytic series solution to the theoretical problem for field representations of rotationally symmetric anisotropic spheres (where both $\bar{\boldsymbol{\epsilon}}$ and $\bar{\boldsymbol{\mu}}$ are tensors), but also carries out extensive parametric studies of single- and joint-anisotropic effects on scattering behaviors. As far as anisotropic spheres are concerned, dyadic Green's functions for radially multilayered anisotropic spheres, using spherical Bessel functions of fractional order, will be reported in the future. In that case, the source and field points can be arbitrarily located. If the number of total layers becomes 2, it is just the specific case studied in this paper.

ACKNOWLEDGMENTS

The authors are grateful to the support from the SUMMA Foundation for financial support, to the Joint Program offered by the National University of Singapore (in Singapore) and Supélec (in Paris) in terms of financial support by both parties, to the support by a U.S. Air Force Project (No. AOARD-064031), and to the joint project supported by the France-Singapore "Merlion Project."

APPENDIX: SOME PROPERTIES OF RICATTI-BESSEL AND HANKEL FUNCTIONS AND LEGENDRE POLYNOMIALS

In the formulation of potential and field quantities in this paper, spherical Ricatti-Bessel and Hankel functions are employed, and they are defined as follows

$$j_n(x) = \sqrt{\frac{\pi x}{2}} J_{n+1/2}(x) \tag{A1}$$

$$h_n(x) = \sqrt{\frac{\pi x}{2}} H_{n+1/2}(x). \tag{A2}$$

In the calculation of RCS values, the following identities have to be used for simplicity:

$$\frac{\partial j_n(x)}{\partial x} = \frac{j_n(x)}{2x} + \frac{1}{2}[j_{n-1}(x) - j_{n+1}(x)] \tag{A3}$$

$$\frac{\partial h_n(x)}{\partial x} = \frac{h_n(x)}{2x} + \frac{1}{2}[h_{n-1}(x) - h_{n+1}(x)]. \tag{A4}$$

When the argument of the second-order Ricatti-Hankel functions approaches a sufficiently large value, we will have

$$h_n^{(2)}(x) \approx i^{n+1} e^{-ix}, \quad x \to \infty. \tag{A5}$$

For the associated Legendre polynomials, the following properties have been utilized in this paper:

$$\left.\frac{\partial P_n^m(\cos\theta)}{\partial\theta}\right|_{\theta=\pi} = -(-1)^{n-1}\frac{n(n+1)}{2}\delta_m^1 \tag{A6}$$

$$\left.\frac{P_n^m(\cos\theta)}{\sin\theta}\right|_{\theta=\pi} = (-1)^{n-1}\frac{n(n+1)}{2}\delta_m^1 \tag{A7}$$

where δ_m^1 denotes the Kronecker delta function.

[1] M. Kerker, *The Scattering of the Light and Other Electromagnetic Radiation* (Academic Press, New York, 1969).
[2] C. F. Bohren and D. R. Huffman, *Absorption and Scattering of Light by Small Particles* (Wiley, New York, 1998).
[3] W. C. Chew, *Waves and Fields in Inhomogeneous Media* (Van Nostrand, New York, 1990).
[4] W. Ren, Phys. Rev. E **47**, 664 (1993).
[5] A. L. Aden and M. Kerker, J. Appl. Phys. **22**, 1242 (1951).
[6] Z. S. Wu and Y. P. Wang, Radio Sci. **26**, 1393 (1991).
[7] R. J. Tarento, K. H. Bennemann, P. Joyes, and J. Van de Walle, Phys. Rev. E **69**, 026606 (2004).
[8] N. K. Uzunoglu, P. G. Gottis, and J. G. Fikioris, IEEE Trans. Antennas Propag. **33**, 90 (1985).
[9] C. T. Tai, *Dyadic Green's Functions in Electromagnetic Theory*, 2nd ed. (IEEE Press, Piscataway, NJ, 1994).
[10] V. G. Farafonov, N. V. Voshchinnikov, and V. V. Somsikov, Appl. Opt. **35**, 5412 (1996).
[11] O. B. Toon and T. P. Ackerman, Appl. Opt. **20**, 3657 (1981).
[12] I. E. Psarobas, N. Stefanou, and A. Modinos, Phys. Rev. B **62**, 278 (2000).
[13] R. P. Devaty, Phys. Rev. B **38**, 7972 (1985).
[14] G. W. Ford and S. A. Werner, Phys. Rev. B **18**, 6752 (1978).
[15] L. W. Li, J. H. Koh, T. S. Yeo, M. S. Leong, and P. S. Kooi, IEEE Trans. Geosci. Remote Sens. **37**, 1967 (1999).
[16] L. W. Li, C. K. Lee, T. S. Yeo, and M. S. Leong, Electromagnetics **22**, 235 (2002).
[17] J. B. Titchener and J. R. Willis, IEEE Trans. Antennas Propag. **39**, 35 (1991).
[18] J. C. Monzon, IEEE Trans. Antennas Propag. **35**, 670 (1987).
[19] M. A. Hasan and P. L. E. Uslenghi, IEEE Trans. Antennas Propag. **38**, 523 (1990).
[20] L. W. Li, S. H. Liu, M. S. Leong, and T. S. Yeo, IEEE Trans. Microwave Theory Tech. **49**, 1361 (2001).
[21] Y. L. Geng, X. B. Wu, L. W. Li, and B. R. Guan, Phys. Rev. E **70**, 056609 (2004).
[22] C. W. Qiu, L. W. Li, Q. Wu, and T. S. Yeo, IEEE Antennas Wireless Propag. Lett. **4**, 467 (2005).
[23] R. D. Graglia, P. L. E. Uslenghi, and R. S. Zich, Proc. IEEE **77**, 750 (1989).
[24] J. I. Dadap, J. Shan, K. B. Eisenthal, and T. F. Heinz, Phys. Rev. Lett. **83**, 4045 (1999).
[25] V. V. Varadan, A. Lakhtakia, and V. K. Varadan, IEEE Trans. Antennas Propag. **37**, 800 (1989).
[26] R. G. Newton, *Scattering Theory of Waves and Particles*, 2nd ed. (McGrow-Hill, New York, 2002).
[27] J. C. Monzon, IEEE Trans. Antennas Propag. **37**, 728 (1989).
[28] J. E. McDonald, Q. J. R. Meteorol. Soc. **88**, 183 (1962).